



HAL
open science

Rock magnetic analyses as a tool to investigate diversity of drift pumice clasts: An example from Japan's 2021 Fukutoku-Oka-no-Ba (FOB) eruption

Julie Carlut, Aude Isambert, Claire Carvallo, Geoffrey Garcia da Fonseca, Nelly-wangue Moussissa, Arthur Bouis, Kenta Yoshida

► To cite this version:

Julie Carlut, Aude Isambert, Claire Carvallo, Geoffrey Garcia da Fonseca, Nelly-wangue Moussissa, et al.. Rock magnetic analyses as a tool to investigate diversity of drift pumice clasts: An example from Japan's 2021 Fukutoku-Oka-no-Ba (FOB) eruption. *Island Arc*, 2024, 33 (1), pp.e12507. 10.1111/iar.12507 . hal-04398181

HAL Id: hal-04398181

<https://hal.science/hal-04398181>






Submitted on 16 Jan 2024

HAL is a multi-disciplinary open access archive for the deposit and dissemination of scientific research documents, whether they are published or not. The documents may come from teaching and research institutions in France or abroad, or from public or private research centers.

L'archive ouverte pluridisciplinaire **HAL**, est destinée au dépôt et à la diffusion de documents scientifiques de niveau recherche, publiés ou non, émanant des établissements d'enseignement et de recherche français ou étrangers, des laboratoires publics ou privés.

RESEARCH ARTICLE

Rock magnetic analyses as a tool to investigate diversity of drift pumice clasts: An example from Japan's 2021 Fukutoku-Oka-no-Ba (FOB) eruption

Julie Carlut¹  | Aude Isambert¹  | Claire Carvalho²  |
Geoffrey Garcia da Fonseca¹  | Nelly-Wangue Moussissa¹  | Arthur Bouis¹ |
Kenta Yoshida³ 

¹Université Paris Cité, Institut de Physique du Globe de Paris, CNRS UMR-7154, Paris, France

²Institut de Minéralogie et de Physique des Milieux Condensés, Sorbonne Université, Paris, France

³Research Institute for Marine Geodynamics, Japan Agency for Marine-Earth Science and Technology, Yokosuka, Japan

Correspondence

Julie Carlut, Université Paris Cité, Institut de Physique du Globe de Paris, CNRS UMR-7154, 1 rue Jussieu, 75238 Paris Cedex 5, France.
Email: carlut@ipgp.fr

Funding information

Centre National de la Recherche Scientifique; Institut de Physique du Globe de Paris; Japan Society for the Promotion of Science, Grant/Award Number: JP19K14825

Abstract

The crystallization of nanolites within magma chambers has recently raised a strong interest due to their impact on increasing melt viscosity and triggering magmatic eruptions. In 2021, the Fukutoku-Oka-no-Ba (FOB) underwater eruption produced large quantities of pumices that eventually formed rafts drifting at the surface of the ocean to the East coasts of Japan. Pumices collected along the shore shortly after grounding show various colors, microscopic and Raman analyses made by Yoshida et al. (*Island Arc*, 31, 1, 2022) revealed the presence of magnetite nanolites in some of them. In this study, we explore the magnetic properties of a batch of pumices of different colors from the FOB eruption, aiming to refine characterization of iron oxide nanolites. We used various analytical techniques such as SEM and FEG-SEM observations, EDS-X analyses, and rock magnetic experiments, including thermomagnetic analyses, hysteresis curves, coercivity analyses and FORC measurements. Our findings reveal that the iron oxides present in the FOB samples are Ti-magnetite, with minor amounts of Mg and Al. The magnetic crystals show a wide range of sizes, from extra small iron oxide nanolites (ESION) in the pumices with the lighter colors, to more bulky grains reaching the micrometer size in some of the dark color samples, significant diffusion is inferred in that case. Consequently, the magnetic characterization of iron oxide crystals within the Fukutoku-Oka-no-Ba pumices reveals varying stages of nucleation, dissolution, growth, and diffusion processes, providing evidences for the heterogeneous state of the magma during the eruption.

KEYWORDS

eruption, Fukutoku-Oka-no-Ba, magnetic nanoparticles, nanolite, pumice, rock magnetism

This is an open access article under the terms of the [Creative Commons Attribution-NonCommercial](https://creativecommons.org/licenses/by-nc/4.0/) License, which permits use, distribution and reproduction in any medium, provided the original work is properly cited and is not used for commercial purposes.

© 2023 The Authors. *Island Arc* published by John Wiley & Sons Australia, Ltd.

1 | INTRODUCTION

Between August 13th and 16th, 2021, the Fukutoku-Oka-no-Ba (FOB) volcano, situated about 5 km northeast of Minami-Ioto Island (Japan), erupted in a Plinian event, spewing large quantities of pumice into the sea that eventually formed a pumice raft in the ocean (Maeno et al., 2022; Yoshida et al., 2022). The FOB volcano is part of a vast underwater volcanic complex covering approximately 450 km². This eruption is the fourth that has been recorded at this complex over the past 40 years (Yoshida et al., 2022). Following the eruption, the pumice raft drifted at the surface of the sea for >1000 km and reached several locations along the East coast of Japan during October and November 2021. Several pumice samples could be collected soon after their arrival from the Nansei islands, and their textural and geochemical analyses were reported in Yoshida et al. (2022). The pumices were classified into different types based on the texture and color of the matrix. The samples ranged from dark tones (black type) to light ones (gray type) (see Yoshida et al., 2022). The whole rock chemical composition analyses made on the different types of samples gave identical results, eliminating bulk chemistry as a cause for the color difference. A faint signal of magnetite appeared in the Raman spectrum from the dark type pumices with associated bulk rock susceptibility measurements on the order of 9×10^{-03} SI (cm³/g). This led Yoshida et al. (2022) to infer the presence of magnetite nanoparticles called “nanolites”, which measure just a few nanometers in size, hence too small to be observed by conventional SEM but responsible for the color differences in the samples. The presence of nanolites was later confirmed in one of the dark tone samples by the same authors using TEM and Fe K-edge XANES (X-ray absorption near edge structure) microanalyses (Yoshida et al., 2023). Nanolites crystallization influences magma behavior by increasing melt viscosity and subsequent gas release during volcanic eruptions. Assessing their abundance is, therefore, of high interest (e.g., Di Genova et al., 2020; Yoshida et al., 2023). Magnetic parameters, such as magnetization and magnetic coercivity, offer highly sensitive methods for tracking the nucleation and growth of iron oxides (e.g., Malvoisin et al., 2012). Despite this advantage, only few studies have reported magnetic measurements on pumices (but see the recent study by Knafelc et al., 2022). In this study, we aimed to characterize the magnetic properties of the pumices from the FOB eruption and identify the composition of the magnetic phases, their size and distribution. A correspondence is made between magnetic parameters and pumices color. A specificity of this work is that it was part of a long-term undergraduate student project that aimed to address questions regarding the reproducibility and accessibility of experimental data using a FAIR approach. More information regarding these issues is included in section 4 of this paper and in the online data.

2 | SAMPLES SELECTIONS AND METHODS

Samples were collected during October to December 2021 by Yoshida et al. (2022) on the shore from three localities: Ōshima Island (abbreviated IOKH in the following), located off the coasts of the Izu

peninsula, 100 km south of Tokyo, Amami- Ōshima Island (abbreviated AOAC in the following) located in the Kagoshima Prefecture, some 1100 km southwest of the IOKH location, and Okinawa Island (abbreviated OKI in the following), c.a. 200 km southwest from the AOAC site. Samples were classified by Yoshida et al. (2022) according to color. The gray type (GT) is the most common and represents 90% of the collected samples; it corresponds to a gray colored vesicular glass matrix with black enclaves of millimeters size. The rest of the samples is composed, from light tone to dark tone, of: amber type (AT), brown type (BRT), pale gray type (PGT) and black type (BT). The BT pumices are often combined to GT, sometimes in a streaky manner with distinct bands of each type. For this study, we used a batch of samples from each type collected at AOAC (GT, AT, BRT, PGT, BT), IOKH (GT) and OKI (BT).

To better document the color classification process, we performed a colorimetry analysis on cross sections cut from the samples using a digital camera under a 6400 K light. The resulting average colors within each glassy matrix are associated to the corresponding hexadecimal (HEX) and Hue, Saturation, Lightness (HSL) color codes.

For each pumice type, we picked between 3 and 5 chips, weighting 20 and 60 mg. The chips were selected so that they represent pure glassy part, type without phenocrysts. In addition, ~150 mg of powders was grounded for each sample, once again selecting the purest type. The magnetic susceptibility variations as a function of temperature were measured on the whole powders using an AGICO KLY-3 with a CS-3 heating unit.

Hysteresis measurements and FORC diagrams were performed with a magnetometer (μ -VSM) from Princeton Measurements Corporation at the IGP-IMP-PMC Mineral Magnetism Analytical Facility. The routine measurement parameters for hysteresis were: field up to 1 T, averaging measurement time 100 ms, field increments between 1 and 5 mT, 1 mT for backfield measurements (H_{cr}). IRM curve acquisitions were performed on the same instrument with an increasing induced field following a log distribution of the field steps (with 80–100 steps) up to 1 T. The analysis of the IRM curves was performed following the unmixing approach proposed by Kruiver et al. (2001), Egli (2003), and Heslop et al. (2004). We used the MAX UnMix application (<http://shinyapps.its.carleton.edu/max-unmix/>) (Maxbauer et al., 2016) with an intermediate smoothing factor of 0.5 to determine the different components of coercivity contributing to the IRM. FORC diagrams allow a qualitative characterization of the magnetic domain structure and magnetostatic interactions, by measuring a set of partial hysteresis curves that originate from the descending branch of the hysteresis loop (Pike et al., 1999; Roberts et al., 2000). Magnetic carriers with different domain structures plot in different areas of the diagram, making FORC diagrams a useful tool for fine magnetic characterization. FORC diagrams were each calculated from 125 to 160 individual FORCs (depending on the horizontal extent of the FORC diagram features) measured with a field step of 1.25 mT, at room temperature, and with an averaging time of 0.1 s. Each FORC diagram was subsequently analyzed with the Forcinel software (Harrison & Feinberg, 2008), with a smoothing factor of 5 for the vertical and central ridges and 8 elsewhere (Egli, 2013). The variable smoothing considerably reduces the noise levels by applying larger smoothing factors to the background,

while preserving the areas along the axes with relatively small smoothing factors.

The scanning electron microscope (SEM) and field emission gun scanning electron microscope (SEM-FEG) observations were performed using respectively a Zeiss SEM EVO MA10 and a Zeiss FEG FIB SEM AURIGA 40, both on unpolished gold coated fragments and carbon coated thin sections for GT, BT and PGT pumices.

3 | RESULTS

3.1 | Optical observations

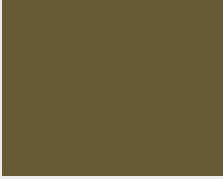

The sample description with photo and color code is given in Table 1. Samples from an identical type give very close color codes and the average color is reported. For 3 of the sample types (BT, PGT, and BRT), the matrix is slightly patchy at the scale of observation (~ millimeter) with two shades, one dominant and the other secondary

(representing ~20% to 50% of the matrix). In that case the reported resultant color is obtained by mixing the dominant and secondary color with respect to their percentage. Colors are given in (HEX) and in (HSL), in this last format the Lightness (L) is a scale from white to black, which allows to assess how dark a color is. Three of the sample types have a dominant color classified as “dark” with lightness of 25% or less (BT, PGT, and BRT). It should be noted that this classification concerns the samples processed in this study for magnetic mineralogy. It is based on the small group of samples to which we had access and may not be representative of all pumices from the FOB eruption. In particular, the PGT-type pumices treated here are particularly dark (see Yoshida et al., 2022).

3.2 | Optical, SEM and FEG observations

Macroscopic observation shows rather friable pumice samples (especially GT samples) with a micro-vesicle type texture (i.e., the vesicles

TABLE 1 Color code in HEX and HSL for the different types of pumice.

Pumice type	Photo	Code HEX 1	%	Code HEX 2	%	Resultant in HEX and HSL	Color
Pale Gray Type (PGT)		#31302B	80%	#464536	20%	#35342D HSL: 52, 8%, 19%	
Black Type (BT)		#2C2A24	80%	#B1AE98	20%	#47443B HSL: 45, 9%, 25%	
Brown Type (BRT)		#373631	50%	#635733	50%	#4D4732 HSL: 47, 21%, 25%	
Amber Type (AT)		#645A34	100%	X	X	#645A34 HSL: 48, 32%, 30%	
Gray Type (GT)		#A39774	100%	X	X	#A39774 HSL: 45, 20%, 55%	

Note: When two shades are present both are reported as Code HEX 1 and Code HEX 2 with their respective percentage, the reported resultant color is obtained by mixing both shades with their percentage.

are typically <1 mm in size). In the case of samples with banded features we note a sharp contrast between GT and BT texture at the millimeter scale with occasional bubbles at the interface (Figure 1a). These samples were avoided for rock magnetic experiments but their occurrence indicate that GT and BT pumices were (at least sometimes) transported together, without re-mixing, in the magma conduit. SEM and FEG observations were made on three of the pumice types, selected for their contrasting color properties: a BT and a PGT of the darkest tone and a GT pumice of light color. Electron microscopic observations of unpolished carbon and/or gold coated fragments show that the bulk of the samples consists of empty vesicles of sub-spherical shapes reminiscent of a “foam” type texture (typically for the BT fragments, see Figure 1c) or more elongated forms (as for the PGT fragments, Figure 1d) revealing some shear stress during formation of this pumice.

Phenocrysts measuring several hundred μm were occasionally observed in the samples (Figure 1b) and carefully avoided when we extracted chips for magnetic measurements. Compositional analyses using an EDS-X show that these phases are pyroxene, plagioclases and titanomagnetites. The titanomagnetites have a small proportion of substitution, the analyzed compositions are close to the formula $\text{Fe}_{3-x-y}\text{M}_y\text{Ti}_x\text{O}_4$, with $x + y = 0.4$ and where M corresponds to a mixture of variable proportion of Al and Mg. These phases, included in the vitreous matrix of the FOB pumices, have also been described by Yoshida et al., 2022.

Observations with a high resolution were performed using a FEG microscope. The observations focused on the glassy edging with a high magnification range (between 2.10^4 and 3.10^4). Under these conditions no compositional heterogeneities could be observed on the GT thin-section and the glassy part is very homogeneous at the FEG scale (see Figure 2a). The BT section is characterized by the presence

of numerous white rounded or rectangular high contrast crystals giving a “snowfall” texture (Figure 2b). Rectangular shaped crystals have a mean size around 100 nm while the smallest rounded shape crystals are rather in the 10–20 nm range. The very small size of the crystals, did not allow to perform accurate EDS-X analysis, but bimodal shape distribution could indicate two different phases. This “snowfall” texture is observed on all BT glassy thin section surface (Figure 2c). In the PGT sample, larger crystals are observed (see example in Figure 2d,e), the glassy matrix is inhomogeneous at the FEG scale with organization in “patches” consisting in zone with higher amount of crystals distributed at a few μm distance from each other. Two types of crystal morphology are observed, small high contrast rounded shape and rectangles or rods with a lower contrast. The EDS-X chemical analysis beam clearly points to iron oxide composition with some titanium for the high contrast phase (Figure 2f) and pyroxene for the slightly lower contrast phase.

3.3 | Rock magnetic results

3.3.1 | Thermomagnetic analyses

The magnetic susceptibility variations with temperature for each type of pumices are illustrated in Figure 3a. The curves exhibit similar shapes with only minor differences. On the heating branch of the curves, there is a gradual increase in susceptibility up to approximately 300°C for all samples, except for BT-AOAC which displays a more pronounced curve with an unclear peak around 120°C. A sharp decline occurs at around 310–320°C. The point of inflection, corresponding to this drop, falls between 318 and 330°C for all samples. Subsequently, there is a moderate increase in susceptibility, reaching

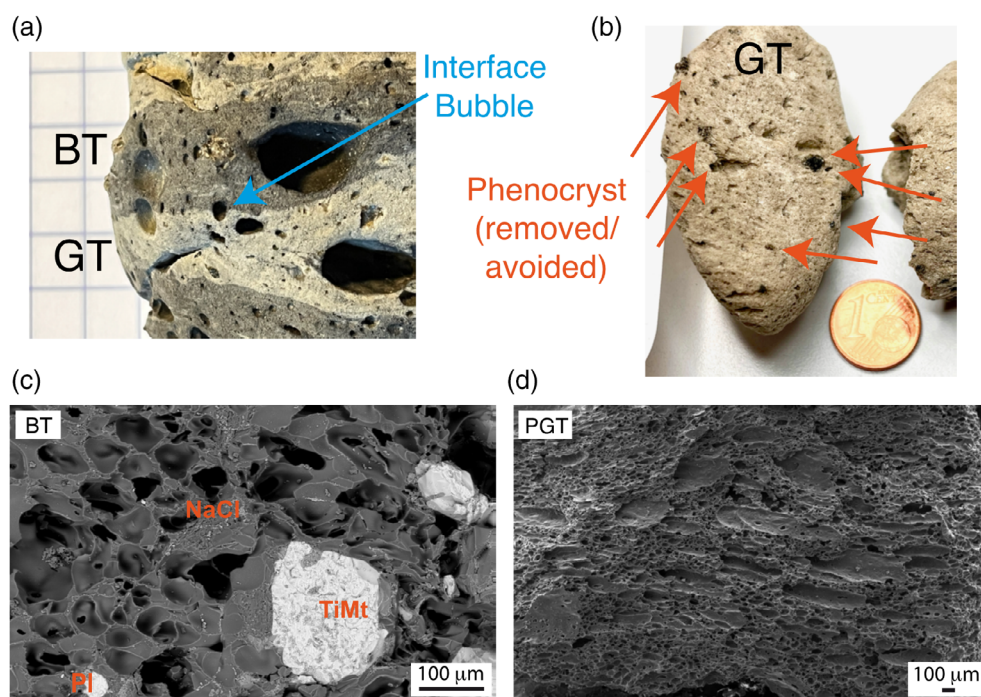
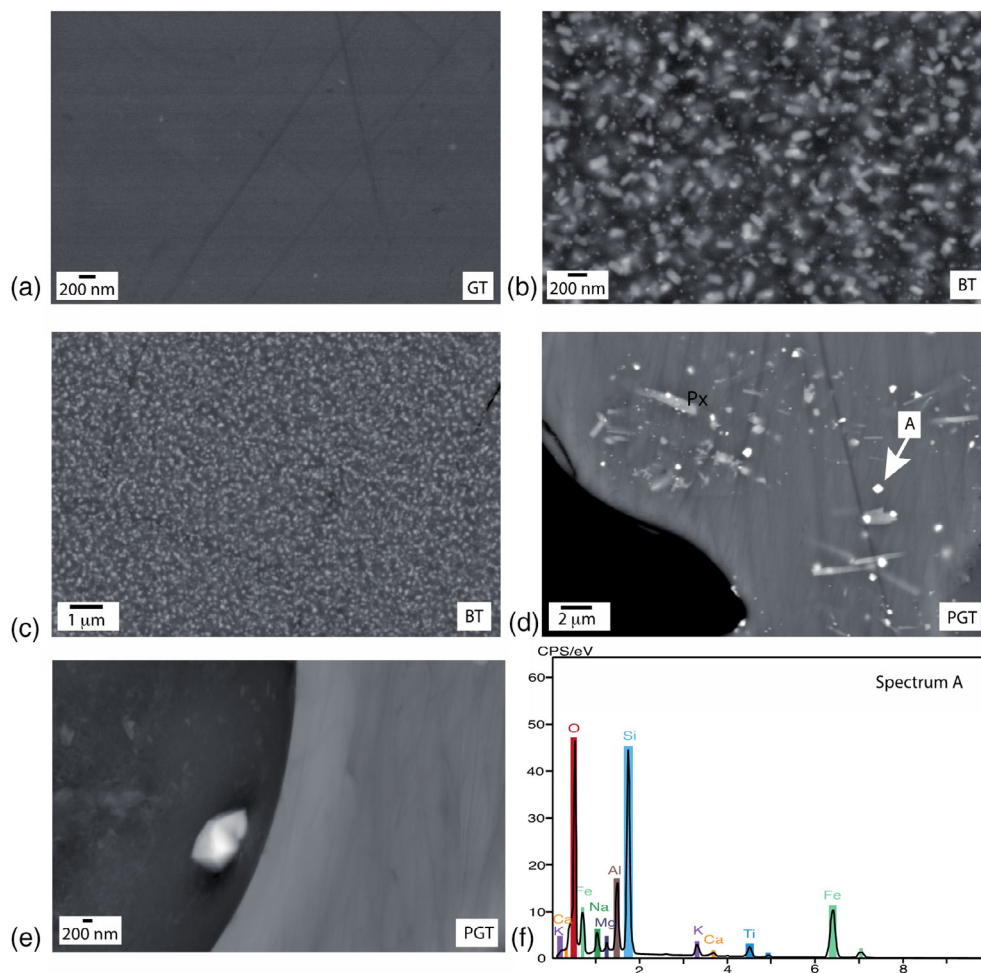


FIGURE 1 Pumice fragments (a) fragments showing a mixing between GT and BT type with bubbles at the interface (b) A GT pumice showing pristine glassy matrix and phenocrysts (orange arrow), the phenocrysts were avoided and/or removed from the specimens (c) fragments under the SEM showing the glassy texture of a black type with plagioclase and Ti-magnetite phenocrysts (and NaCl crystals from sea water) (d) fragment of a PGT type under the SEM showing elongated texture.

FIGURE 2 (a) Gray type: the texture is homogeneous, the thin spots are associated to particles resting on the surface (b) Black type: a dense population of crystals is observed. (c) Black type: larger scale (d) PGT type: larger crystals emerge (e) PGT type: a crystal grow out of a vesicle surface (f) Composition analysis of a highly contrasted rounded crystal in PGT (point A in d).



a maximum around 415°C in all samples except for AT-AOAC, the maximum is less pronounced for PGT-AOAC. This peak likely indicates the formation and demagnetization of a new magnetic phase formed during heating. Beyond 450°C, there is almost no signal, except for PGT-AOAC which shows a smoother decrease compared to the other samples and still exhibits some signal until 680°C. Lastly, all curves show a strong irreversibility (not shown here).

The decrease starting around 310°C could be caused by the demagnetization of Ti-magnetites reaching their Curie temperature. An alternative explanation is that it corresponds to the destabilization temperature of an unstable magnetic phase (as could be observed in the case of cation deficient Ti-magnetite for instance). In order to decide between the two options the BT-AOAC sample was subjected to consecutive heating cycles, reaching maximum temperatures of 326, 347, and finally 391°C. This process aimed to examine any irreversibility that would indicate a chemical transformation taking place. The curve shows an excellent reversibility until 347°C, there is no indication of chemical destabilization up to this temperature (Figure 3b). The sharp decrease in signal amplitude around 320°C is thus likely due to a Ti-magnetite phase. In the last heating step up to 391°C the signal increases, the cooling branch of the curve shows marked irreversibility attesting for the creation of a new phase at the expense of the Ti-magnetite, as attested by the lower amplitude of

the signal when cooled below 330°C. Such irreversibility and the formation of new phases mask the identification of other phases that could be present before the heating.

3.3.2 | Hysteresis measurements: The hysteresis curves shape

The selection of samples was conducted through visual inspection using a binocular to ensure they had a glassy appearance and were free from visible inclusions or phenocrysts. The hysteresis curves were measured up to 1 T, but only data up to 300 mT are presented to focus on documenting the remanence more effectively. The curves exhibit distinct characteristics, as depicted in Figure 4 for typical samples.

The GT and AT glassy samples show curves that can be overlapped with very weak remanence or coercivity, indicative of a superparamagnetic (SP) behavior (Figure 4a). The hysteresis loops of the BT glassy samples display a constricted middle section, commonly referred to as “wasp-waisted” (Figure 4b). This distinctive feature typically suggests the coexistence of two magnetic components with contrasting coercivities, as described by Roberts et al. (1995) (see also Tauxe et al., 1996). In contrast, the BRT and PGT samples exhibit hysteresis curves that lack the “wasp-waisted” characteristic.

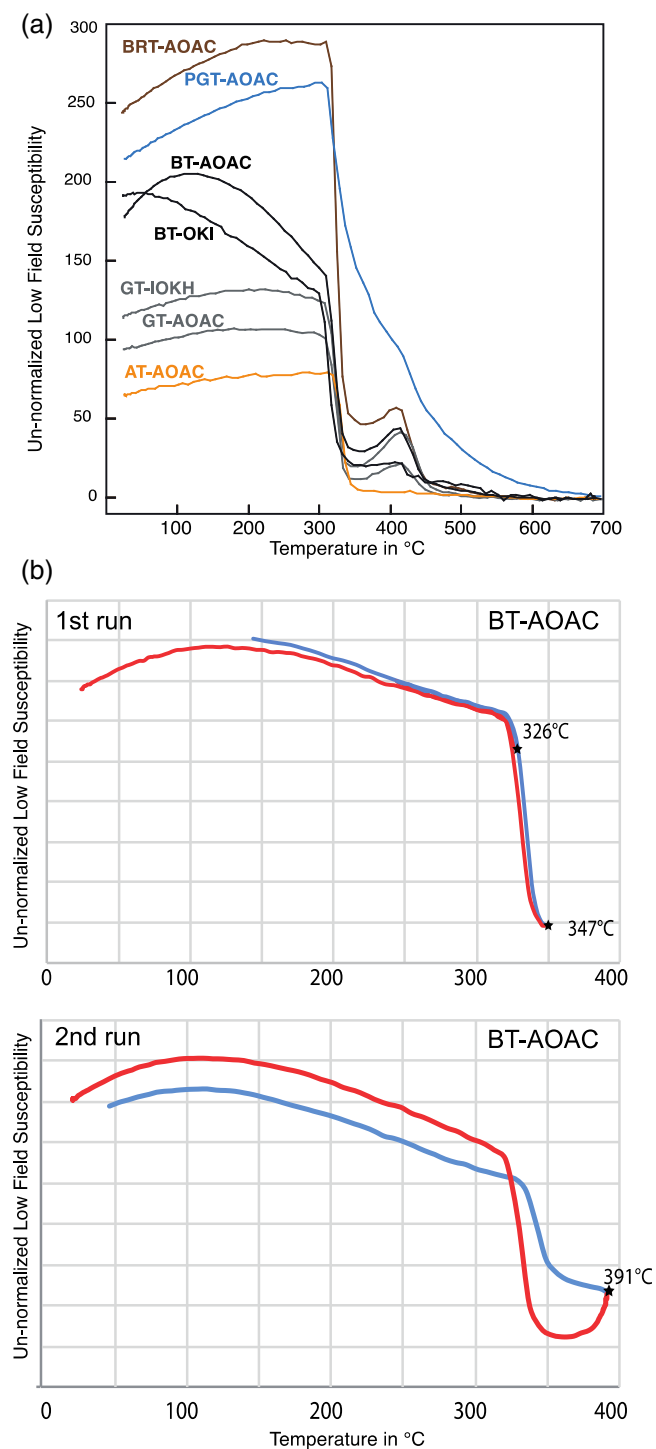


FIGURE 3 (a) Thermomagnetic curves for all samples (heating leg) (b) test at different temperature for BT-AOAC.

3.3.3 | Hysteresis measurements: Analysis of the hysteresis parameters

Average values of the hysteresis parameters and their standard deviation were calculated and given in Table 2. Results are presented on Figure 5 along with the type of the pumice in the following order: GT, AT, BT, BRT and PGT. The mean saturation magnetization (M_s) of the

samples increases from around $0.15 \text{ Am}^2/\text{kg}$ up to $0.86 \text{ Am}^2/\text{kg}$ (see Figure 5a). The remanent magnetization after saturation (M_{rs}) ranges from around 2×10^{-3} to $0.1 \text{ Am}^2/\text{kg}$ (see Figure 5b). GT and AT give the lowest M_{rs} values in line with their “paramagnetic-like” hysteresis curves. The increase of the remanence in BT, BRT and PGT reflects the growing openness of the hysteresis curves. The coercive field (H_c) is very low for GT and increases up to the PGT samples (Figure 5c). The coercive forces (H_{cr}) show an interesting pattern with a maximum for BT and BRT with mean values around 50 mT and large scatter, the values for the PGT chips are clustered around a mean of 43.4 mT with a SD of ~ 1 mT only (Figure 5d).

3.3.4 | IRM acquisition curves

IRM acquisition curves were acquired for all sample types. The data proved to be quite noisy for GT and AT, due to their low remanence, as indicated by the gray dots (Figure 6a). No meaningful unmixing of these data could be achieved even with a high smoothing parameter. In contrast, it has been possible to successfully unmix BT, BRT, and PGT acquisition curves with two distinct components, denoted as B1 and B2 (Figure 6b–d). The major component, B1, exhibited variations ranging from 117 mT in BT to 87 mT in BRT and 59 mT in PGT. The secondary component, B2, displayed a range of 17–46 mT, we note that its reproducibility, when MaxUnmix was used with slightly different starting parameters, was unsatisfactory, raising questions about its significance. This component might be explained by the reduced coercivity of particles approaching the SP/SD boundary, and/or by the interactions between individual grains.

3.3.5 | FORC diagrams

FORC diagrams were performed on one specimen of each type and were plotted with identical smoothing parameters on vertical and horizontal scales (Figure 7). Samples GT and AT, for which hysteresis loops were SP-like, show a FORC distribution peak at the origin of the diagram and contours that are almost vertical, which is characteristic of a SP behavior. A faint extension of the lowest contour along the horizontal axis is visible for sample AT. This feature becomes stronger for samples BT and especially BRT, and can be interpreted as the sign of a contribution from a non-interacting single-domain (SD) population which becomes more and more important, with a coercivity distribution extending up to about 80 mT for sample BRT. Finally, the FORC diagram for sample PGT clearly shows the presence of two distinct contributions: the SP contribution with a peak at the origin of the diagram and the SD contribution with a peak centered around 40 mT but extending from 20 to 80 mT. For these last two samples, the SP contribution was not visible on hysteresis loops, dominated by a SD signal. In summary, the magnetic grain size shows a very clear progression from SP to SD for samples in the following order: GT, AT, BT, BRT and PGT.

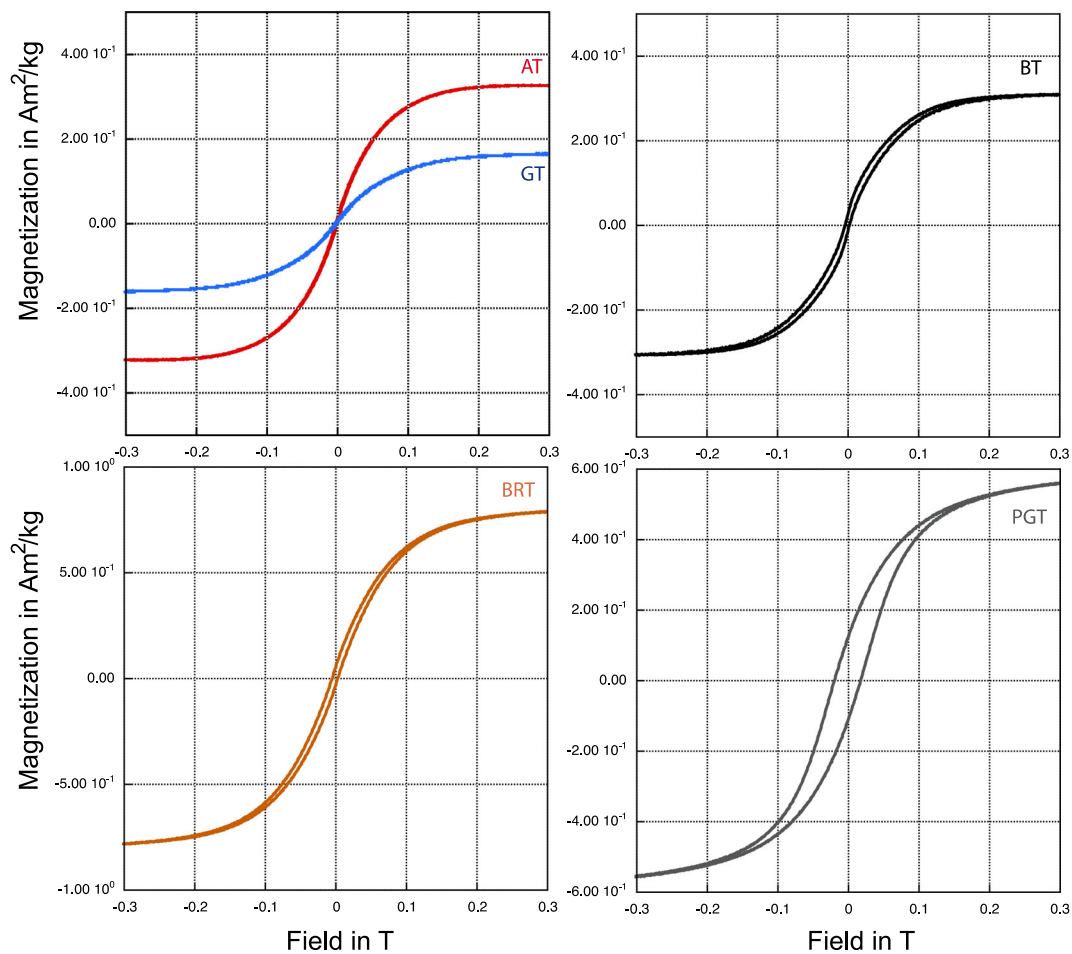


FIGURE 4 Hysteresis curves zoomed in the $[-300 \text{ mT}; +300 \text{ mT}]$ field limit.

TABLE 2 Hysteresis mean values, all means are given with their associated standard deviation (StdD).

TYPE	M_{rs} (Am^2/kg)	StdD (Am^2/kg)	M_s (Am^2/kg)	StdD (Am^2/kg)	H_{cr} (T)	StdD (T)	H_c (T)	StdD (T)
GT	2.04E-03	8.07E-04	1.56E-01	1.01E-01	1.23E-02	3.91E-03	1.18E-03	3.19E-04
AT	4.65E-03	2.03E-03	2.40E-01	1.35E-01	1.44E-02	2.35E-03	1.68E-03	3.69E-04
BT	2.00E-02	9.03E-03	5.11E-01	2.24E-01	4.94E-02	2.06E-02	2.36E-03	1.06E-03
BRT	3.89E-02	7.44E-03	5.23E-01	2.10E-01	5.06E-02	8.89E-03	6.93E-03	3.21E-03
PGT	1.08E-01	1.39E-02	8.63E-01	2.43E-01	4.34E-02	1.11E-03	1.08E-02	5.68E-03

4 | VISUALIZING THE DATA IN A FAIR APPROACH

The acronym FAIR stands for “Findable, Accessible, Interoperable, and Reusable.” This principle comprises a set of recommendations with the objective of enhancing the accessibility, comprehensibility, and utility of scientific data for both the scientific community and the general public (Wilkinson et al., 2016). In adherence to this guideline, the data from this study has been incorporated into a collection of tables and interactive diagrams, which can easily be found online using provided links. Tables are

in tabulated text and interactive diagrams in html format. Note that the html figures can be downloaded and re-opened with a web browser so users can interact with the diagrams to explore the data in more depth, such as by zooming, clicking, or hovering over elements to reveal or hide certain components. All the informations associated with the diagrams (captions, descriptions, sources, etc.) can be obtained from the diagram itself. Finally, all the underlying data for the diagrams can be extracted since they were treated using the open-source Python software and specifically Plotly, an open-source interactive data visualization library for Python, R, Julia, Javascript, ggplot2, F#, MATLAB[®], and Dash.

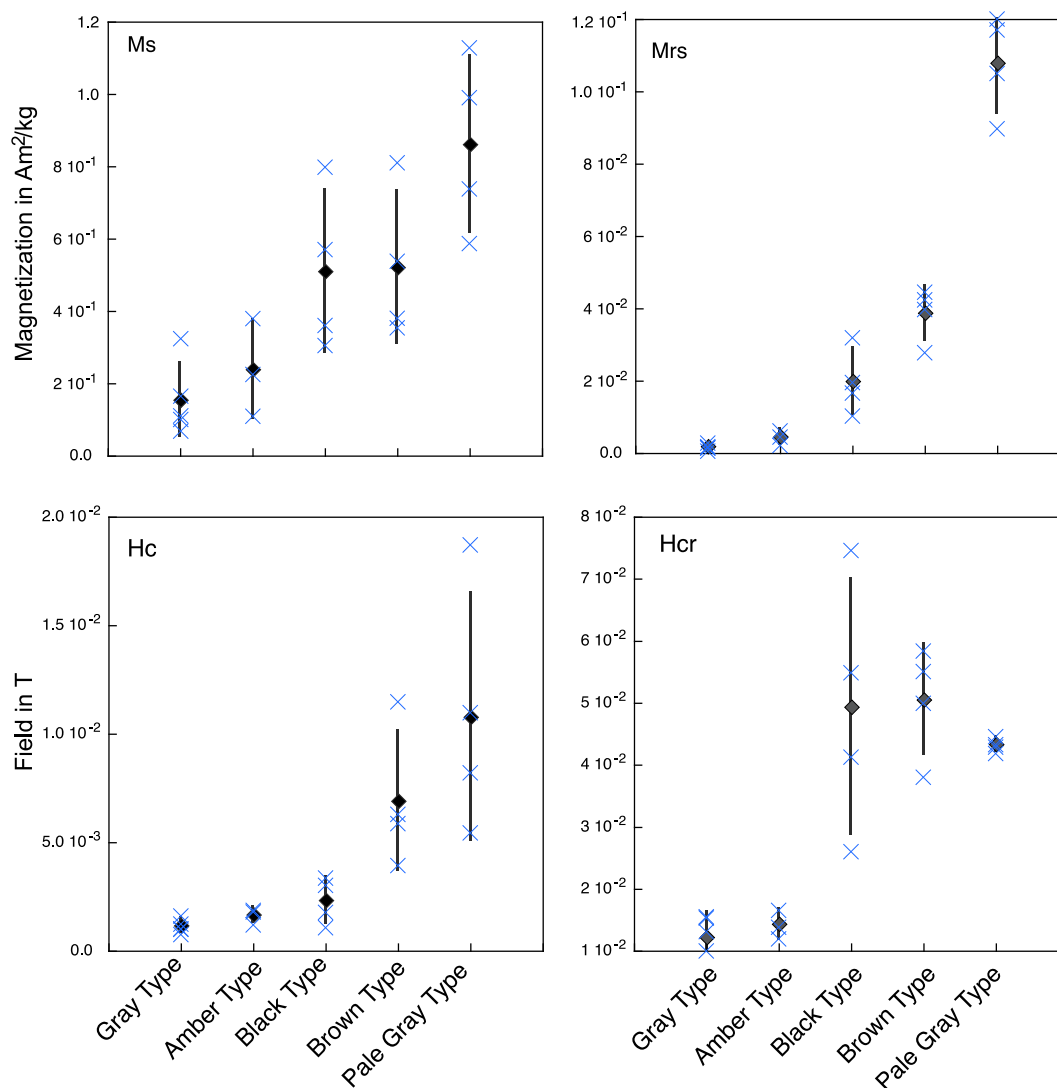


FIGURE 5 Hysteresis parameters (mean values and standard deviation). The values determined for each specimen are depicted as blue dots.

These resources can be accessed at the following location:
<https://doi.org/10.18715/IPGP.2023.lndb1d3z>.

5 | DISCUSSION

5.1 | The iron oxides chemical composition

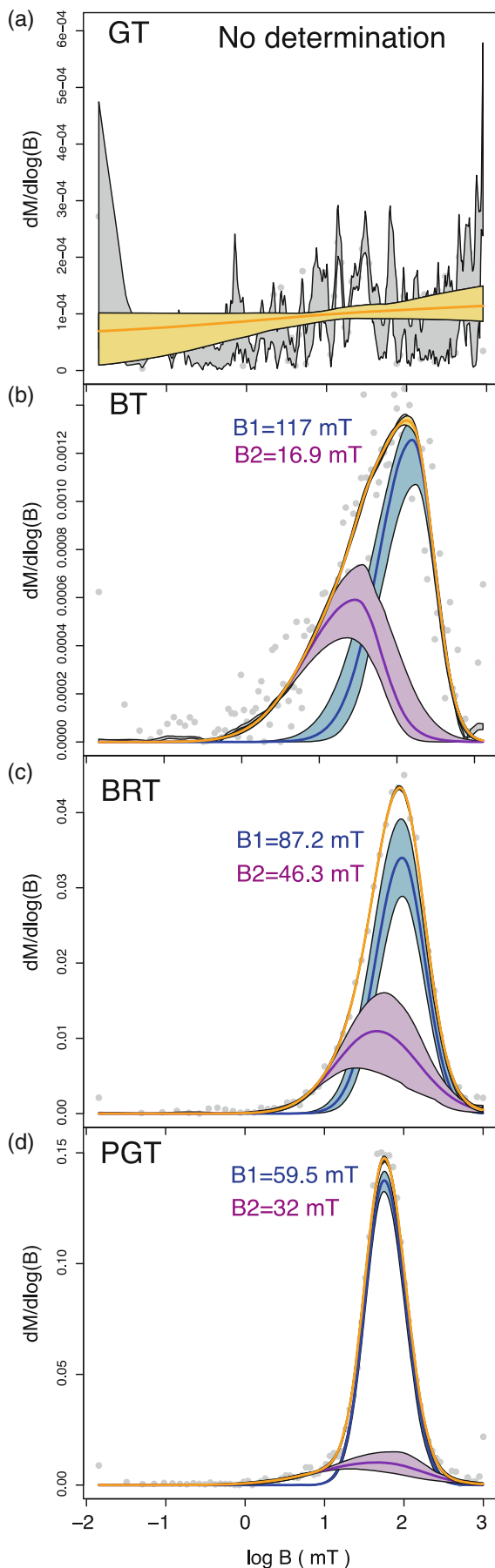
Microscopic examinations of the FOB pumices have revealed the presence of two distinct populations of iron oxides. The first population, observed in all types of pumices, consists of rare and massive Ti-magnetite crystals, measuring several hundreds of micrometers in size and containing minor amounts of Mg and Al. The second population is observed in PGT and BT pumices at very high resolutions using a FEG-SEM (Figure 2b–e) and a Transmission Electron Microscope (TEM) (as discussed in Yoshida et al., 2023).

The focus of this study is on the latter population, which consists of iron oxide grains typically smaller than a micrometer and embedded

within the glassy matrix. However, determining their chemical composition is challenging due to their small size. Through the analysis of Energy Dispersive X-ray Spectroscopy (EDS-X), the small crystals in PGT, displaying rounded or cubic shapes, are identified as iron oxides with some Ti (Figure 2f). Assessing the contributions of Mg and Al is difficult since these elements are also present in large amounts in the surrounding glassy matrix and cannot be specifically attributed to the iron oxides.

For even smaller grains, such as those observed in the BT sample with sizes around 10–20 nm, the analysis capability of the FEG-SEM is reaching its limits. However, observations at the TEM scale (described in Yoshida et al., 2023) and Raman spectroscopic analysis suggest the presence of nano-scale magnetite mixed with larger (~100 nm) biotite crystals.

By turning to the results of the thermomagnetic susceptibility experiments it is possible to estimate more precisely the nature of the carriers of the magnetic susceptibility. Given that powdered samples were prepared exclusively from the glassy regions without the



presence of any visible phenocrysts as illustrated in Figure 1b, it is presumed that the thermomagnetic curves predominantly reflect the magnetic constituents that are part of the glassy matrix. All samples carry magnetic particles which behave in the same fashion with a sharp decrease between 318 and 330°C (see Figure 3a). By referring to studies in which the dependence between substitutions and Curie temperatures is explored (e.g., Akimoto et al., 1957; Clark, 1997) it is possible to propose a composition for the iron oxides. The average Curie temperature value (with a mean at $\sim 323^\circ\text{C}$) found for the main susceptibility carrier in all samples corresponds to a magnetite substituted with Ti in the following amount: $\text{Fe}_{2.6}\text{Ti}_{0.4}\text{O}_4$ (see Figure 8). Substitutions by Al and Mg cannot be ruled out in our samples, Curie temperature of magnetite decreases with Al and Mg substitution in a similar fashion than with Ti, although Al substitution has a subtler effect on the magnetic properties of magnetite (Jiang et al., 2016). We therefore favor a more general formula for the main carrier of the form $\text{Fe}_{2.6}\text{M}_y\text{Ti}_x\text{O}_4$ where M corresponds to a mixture of variable proportion of Al and Mg and $x + y = 0.4$. Interestingly, the level of substitution is identical to that established using EDS-X and microprobe analyses on the large phenocrysts observed on the samples. It is not excluded that a population of less substituted magnetite also exists, since chemical transformation during the heating process prevents to fully explore the thermomagnetic signature of the pristine samples (Figure 3b). In any case, if it exists, this population is not dominant. Another piece of evidence indicating the presence of substitution within the smaller fraction of iron oxide grains comes from the IRM acquisition analyses (see Figure 6). Large titanomagnetite grains exhibit remanent coercivity values within the range of 11–13 mT with no dependence on composition as established by Day et al. (1977). In contrast, remanent coercivity of fine titanomagnetite grains displays a strong compositional dependency with increasing remanent coercivities when compositional parameter (x) rises from 0 to 1. Values exceeding 100 mT are found in fine titanomagnetite grains with a compositional parameter (x) above 0.3 (Day et al., 1977). It is interesting to note that fine-grained, unsubstituted magnetite, such as that found in magnetosomes, exhibits remanent coercivity values that reach only around 70 mT. Consequently, the outcomes of the IRM acquisition unmixing analyses in BT, BRT and to a less extent PGT strongly suggest the presence of a population of fine grains of titanomagnetite with significant substitutions.

Hence, our data suggest that 1/all samples carry an iron oxides population embedded within the glassy matrix 2/this population has a homogeneous composition with identical degree of substitution, Ti is the main substitution cation but we cannot exclude Mg and Al as contributors 3/the larger Ti-magnetite phenocrysts have

FIGURE 6 Unmixing of IRM acquisition curves using the program MAX UnMix (Maxbauer et al., 2016). Gray dots represent the IRM data and yellow curves the smoothed model. The blue curves and purple represent the contribution of respectively the major and minor coercivity component with their 95% confidence intervals (shaded areas). (a) GT type, (b) BT type, (c) BRT type and (d) PGT type.

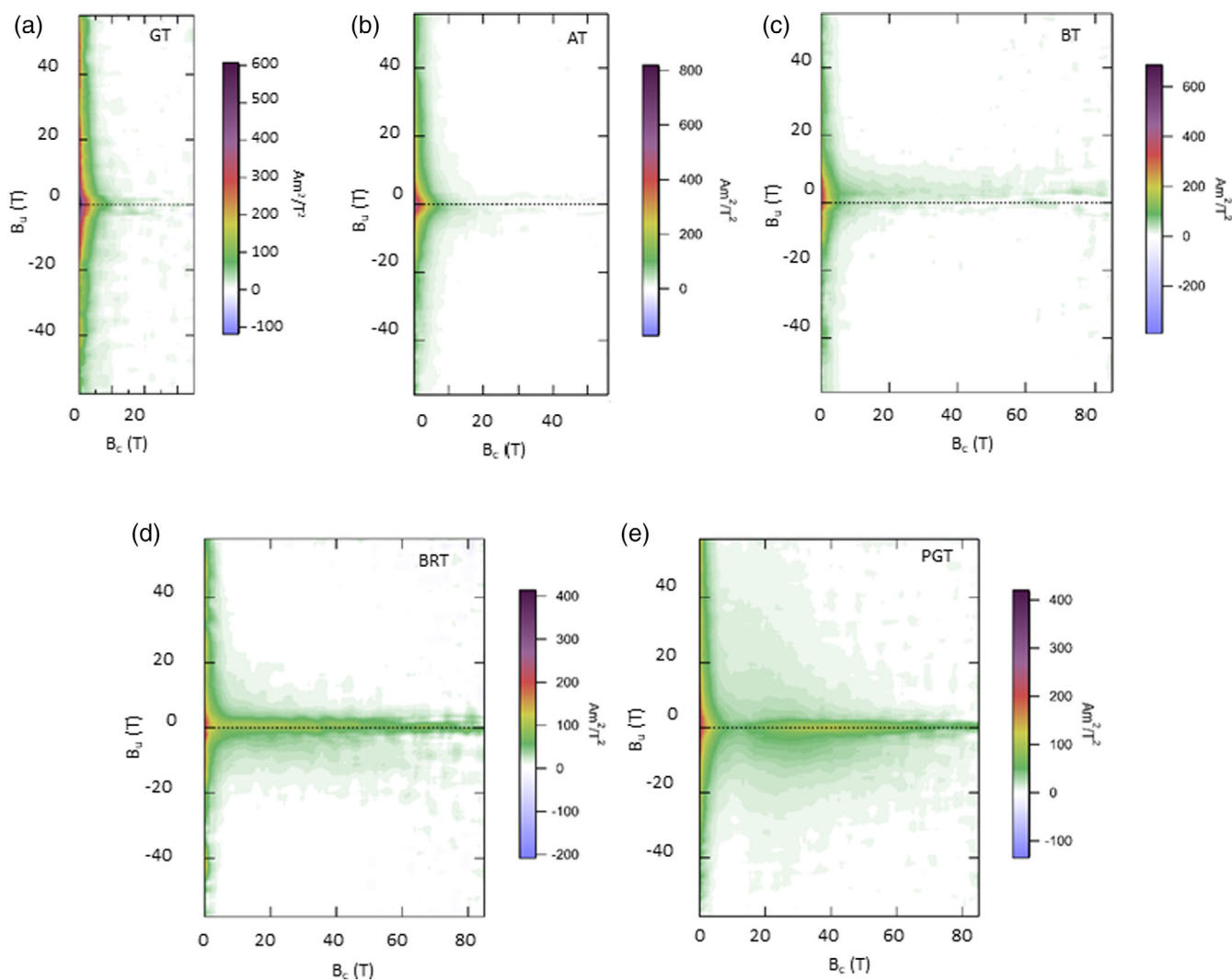


FIGURE 7 FORC diagrams (from left to right: GT, AT, BT, BRT, PGT).

the same degree of substitution, with a significant contribution of Mg and Al cations.

The substitutions occurring in Ti-magnetite are highly influenced by factors such as the composition of the melt, oxygen fugacity, and temperature (Mollo et al., 2013). Consequently, our findings suggest that both the nanosized iron oxides and the larger phenocrysts crystallized from the same melt composition and under similar conditions, at least within the limits of iron oxides composition sensitivity. However, an unresolved question pertains to the precise ratio between Al + Mg and Ti. Experimental studies have demonstrated that basaltic melts rapidly cooled from high temperatures lead to the formation of Ti-magnetite with a higher Al + Mg content and lower Ti content (Mollo et al., 2013). In the case of the FOB pumice, the nanosized crystals within the glassy matrix are expected to have formed through rapid quenching, the larger phenocrysts may have experienced a longer equilibration time. Yoshida et al. (2023) propose that nanolite formation process was provoked by oxidation in the magma chamber. How close in time this process is from the eruption and how far from equilibrium are the newly formed

nanolites may be a fundamental parameter to explore using (Al + Mg) versus Ti ratio. Determining the exact composition of the nano-oxides and their ratio would thus be very valuable for a better understanding of the eruption timing with respect to iron oxides crystallization. However, this specific analysis falls beyond the scope of this paper.

5.2 | A high sensitivity tool to assess the existence and size of magnetite nanolites

Single domain state in magnetite occurs over a range of particle sizes exceeding ~ 20 nm (e.g., Muxworthy & Williams, 2009), above this threshold H_c and M_{rs} increase both sharply and magnetite particles have strong remanence properties. Below ~ 20 nm the particles are in the SP state and do not show remanence, both measured H_c and M_{rs} are then zero. With decreasing size, typically below 3 nm, we enter the domain of the “extremely small iron oxide nanoparticles” (ESIONs, e.g., Kim et al., 2011). Studies indicate that at this scale grains behave

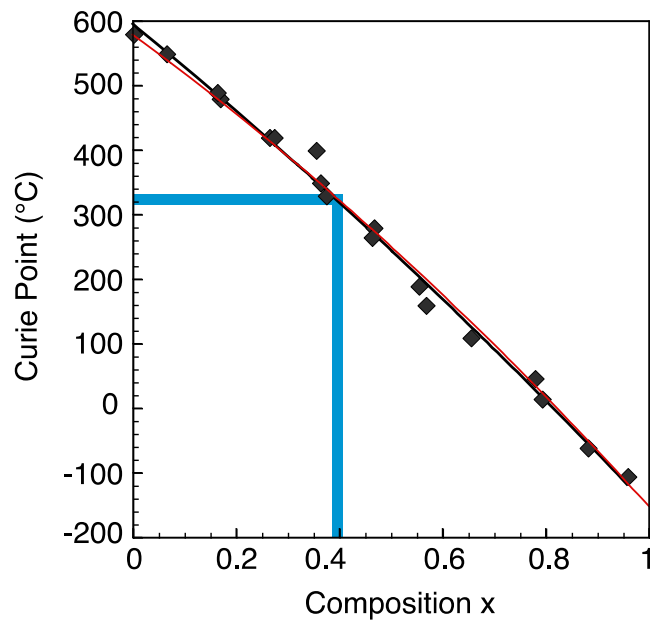


FIGURE 8 Composition determined after Curie temperature based on data from Akimoto et al. (1957) and the equation proposed by Clark (1997).

as core/shell structures with a magnetic core and a magnetically deteriorate outer layer with a canted magnetic spin (e.g., Linderoth et al., 1994). This leads to a decrease of the magnetic moment (Kim et al., 2011; Roca et al., 2006), below a crystal size of 1.5 nm experiments show that the field-dependent magnetization (M_s) decreases of at least one order of magnitude compared to 3 nm size crystals (Kim et al., 2011). Finally, the magnetite lattice parameter ($a = 0.84$ nm) can be considered as the lowest size limit for nano iron oxides population.

In the FOB pumices both, GT and AT, have very low remanence (M_{rs}) and coercivity (H_c) values (see Figure 5). Still, the hysteresis curves depict well define behavior owing to a M_s with a mean in the range of 0.1 (for GT) to 0.3 Am^2/kg (for AT). This behavior could be indicative of a mostly SP population of (titano)-magnetite in the nanometric range as also shown by the FORCs diagrams analyses (Figure 7). Slightly higher values for H_c and M_s for AT indicate slightly larger particles size in this sample. Extensive observations of the GT matrix conducted across a substantial part of a 2 cm-scale thin section at the resolution scale of the FEG-SEM (this study) and on few μm using higher resolution TEM by Yoshida et al. (2023), did not allow the detection of iron oxides crystals. This places a strong restriction on the maximum size of iron oxides, which must remain below the detection limits. These limits are estimated to be around 5 nm for our FEG-SEM and an order of magnitude smaller for TEM. However, it is important to note that in the case of TEM, only a small portion of the glassy matrix was observed due to limitations caused by sample preparation. The mean size of the magnetic particles population for GT samples is thus likely in the range of the ESIONs but above the size limit below which the magnetic moment collapses (~ 1.5 nm in pure magnetite, Kim et al., 2011). The mean size of iron oxides in AT

samples is anticipated to be somewhat larger than that in GT samples, given the higher magnetization values. Alternatively, despite the meticulous specimen selection, it cannot be entirely ruled out that a portion of the larger phenocrysts may have contaminated the glassy matrix. While this is not a concern for BT, BRT, and PGT samples due to their high remanence, it could introduce a potential bias in the case of GT in particular. In these samples, a low and relatively consistent level of phenocryst contamination could be responsible for the observed hysteresis behavior. In this scenario, the glassy matrix may be entirely devoid of nano crystals, all the signal being accounted for by the contamination. This alternative scenario does not hold for AT samples since they exhibit remanences (M_{rs}) surpassing those of GT samples. It seems improbable that all AT samples were contaminated to the same degree by phenocrysts and to a slightly higher extent than GT. Therefore, the most plausible explanation is that AT samples contain a population of very fine iron oxide grains, as discussed earlier.

A wasp waisted hysteresis loop is measured for BT (Figure 4b). It has been largely documented since the 90s (e.g., Roberts et al., 1995) that this feature is caused by a mixture of grains of contrasted coercivities with soft and hard components. Another requirement is that the soft coercivity magnetic grains represent an “overwhelmingly large” fraction of the magnetic mineral population (Roberts et al., 1995). Hence, the wasp waisted loop indicates that the magnetite population within BT is composed of a large fraction below the SP-SD threshold with a soft coercivity and a small fraction which sizes grew above the threshold. By growing above the SP-SD transition the coercivity of the grains changes sharply to become hard. Accordingly, M_{rs} increases significantly in BT compared to AT, while H_c is only faintly increasing due to the wasp waisted form of the hysteresis curve (Figures 4 and 5). H_{cr} shows a more dramatic increase since it is highly sensitive to the SD (remanent) part of the signal. Our interpretation is thus that the BT pumices have a rather unusual characteristic for natural samples carrying a magnetic population with sizes at the SP-SD threshold. For titanomagnetite with a composition of $x = 0.4$ calculations following Neel's relaxation equation give a SP-SD size limit value slightly above pure magnetite (a 10 nm increase is proposed in Butler & Banerjee, 1975), hence, the distribution in BT is inferred to be such that most of the particles have a size that lies below ~ 30 nm (for Ti-iron oxides) but a small proportion are above. This result is in full agreement with the TEM observations (Yoshida et al., 2023) where a population of high contrast iron oxides crystals with a mean size around 15 nm was reported (see also Figure 2b).

In the BRT pumice, the dominant behavior is characterized by single domain (SD) particles, as evident from the hysteresis diagram and FORC analysis. This indicates that the SD population has grown, surpassing the superparamagnetic (SP) population, with an average iron oxide size exceeding the SP-SD transition. The magnetic grain size shows a very clear progression in PGT pumices displaying significantly higher M_{rs} and H_c (Figure 5). The size of magnetic particles in PGT, estimated through direct FEG-SEM observations, varies considerably, ranging from a few tens of nanometers to several hundreds of nanometers for the larger grains (Figure 2d,e).

Overall, our findings highlight a substantial variation in the size distribution of nanosized iron oxides among the different pumices. Additionally, their spatial organization differs significantly, with BT pumice exhibiting a dense and ubiquitous distribution, while PGT pumice displays patchy arrangements. A schematic cartoon in Figure 9 provides a summary of the inferred size distribution and the distribution pattern of iron oxides in the samples. It is important to note that the number of particles depicted in the cartoon is arbitrary, as is the chosen normal distribution.

5.3 | Nucleation and growth of iron oxides

Unlike the coercivity, which is strongly dependent on size, the saturation magnetization is, in principle, and given that the size of particles is above a certain threshold (estimated here at around 1.5 nm after Kim et al., 2011), only dependent on the amount (Wt.%) and chemical type of iron oxides. In our set of samples, Ti-magnetite of the same composition is detected in all samples, hence variations in M_s indicates variations in weight% of Ti-magnetite following the relation:

$$\text{Magnetite (weight\%)} = (M_s/M_{s_Ti - \text{magnetite}}) \times 100 \quad (1a)$$

In the case of Ti-magnetite with substitution in the amount discussed above, the normalizing factor is (O'Reilly, 1984):

$$M_{s_Ti - \text{magnetite}} \sim 50 \text{ Am}^2/\text{kg} \quad (1b)$$

The mean M_s (Table 2) is then used in Equation (1a) to estimate the amount of Ti-magnetite for all our samples. We found ~ 0.3 wt% of iron oxides in GT and ~ 0.5 wt% in AT. It should be noted that these values may be slightly underestimated, especially for GT, if the M_s value is associated with ESION exhibiting strong core/shell effects. Mostly identical M_s are measured for BT and BRT and correspond to an increase up to near ~ 1 wt% of iron oxides for both samples. Finally, the value reaches ~ 1.7 wt% for PGT.

One remaining question concerns the maximum amount of iron oxides that could potentially be attained. A clear limitation is the depletion of iron (and titanium) due to the growth of previously nucleated crystals. According to the mean values from whole rock analyses, the Fe_3O_4 content in the pumices is approximately 3.6 wt% for all samples (Yoshida et al., 2022). This indicates that nearly half of the available iron is utilized by iron oxides in PGT. However, for GT and AT, only around 10%–15% of the available iron is utilized by iron oxides, while for BT and BRT, this percentage increases to 25%–30%.

As a result, all samples contain a significant amount of Ti-magnetite, indicating that the nucleation of iron oxides has occurred in each of them. The total mass of iron oxide is directly related to the number of crystals and to their average volume, which depends on the cube of the average radius of the crystals. Therefore, for samples with a smaller grain size population, the extremely small radius of nanometer-scale crystals must be compensated by a high number of crystals.

A high density of crystals is indeed observed in BT (see Figure 2b,c). This indicates that despite their very small size, the iron

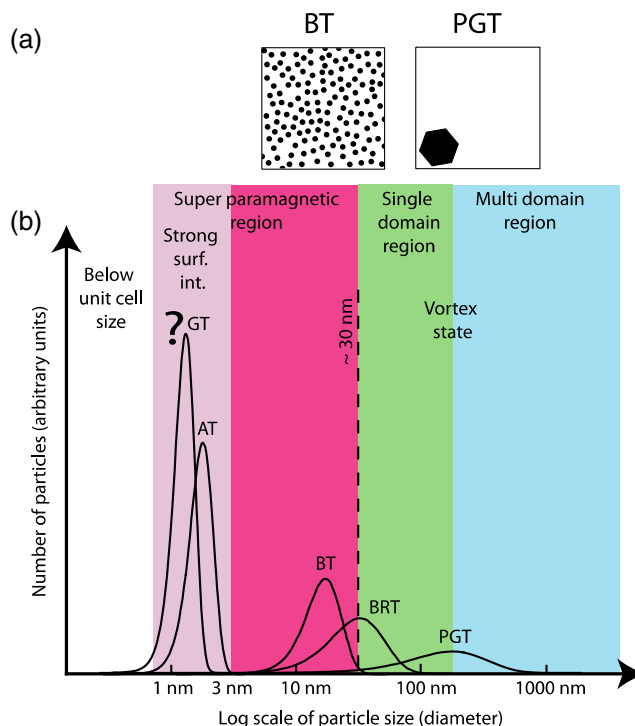


FIGURE 9 Schematic cartoon (not to scale) showing the evolution in size/density of the iron oxide nanoparticles in each pumice type (a) as deduced from the TEM and FEG observations and (b) following the magnetic measurements, a log normal distribution was chosen for the size distribution as typically observed in natural systems. The GT distribution is uncertain as discussed in the text. A distinct region of strong surface interactions (in pink), as identified by a significant decrease in magnetization (see e.g., Kim et al., 2011), is defined within the super paramagnetic range for particle sizes below 3 nm.

oxide crystals can accumulate to a sufficient total mass, as evidenced by the measured weight of 1%. Conversely, for the iron oxide crystal population with larger sizes, the number of crystals must decrease significantly, as observed in PGT, to attain the measured weight percentage values.

Consequently, the occurrence of iron oxide crystals in FOB pumice is governed by two distinct phases. In the first phase, the ubiquitous nucleation and growth of nanocrystals leads to the dense texture, which is observed in BT and suggested by our rock magnetic data in AT and GT (with the caveat mentioned earlier regarding GT).

During another phase, as exemplified by PGT, dissolution recrystallization (Ostwald ripening) and/or the motion of nano-oxides or cations enable aggregation, resulting in the formation of larger, unevenly distributed, iron oxide crystals within the matrix. The specific conditions under which the second phase takes place remain an open question.

5.4 | Color and magnetic properties

The analysis of hysteresis parameters (M_s , M_{rs} , H_c , H_{cr}) has revealed significant variations among the FOB pumice samples. Since the

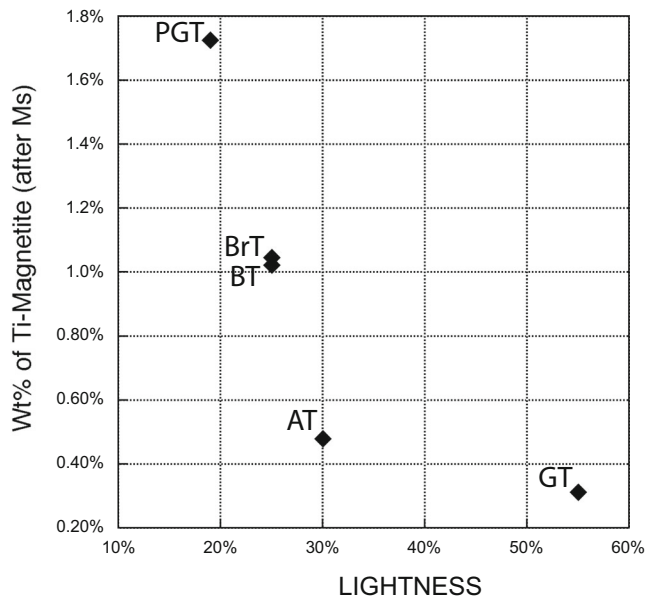


FIGURE 10 Lightness from the HSL color code of the pumices (Table 1) represented versus the Wt% of Ti-magnetite (after Ms).

pumices were classified based on the color of their glassy matrix, we plotted each hysteresis parameter against the Lightness color of the corresponding pumice type. Remarkably, a strong correlation is observed between the Lightness of volcanic pumice glasses and the magnetic properties, as depicted in Figure 10 (shown for M_s). This analysis strongly suggests that the crystallization of iron oxides has a noticeable impact on the color of the glass in FOB pumices. An additional potentially valuable color parameter is the “pink shade”, although not detected in the FOB batch, pink-colored pumices were observed during the Havre 2012 submarine eruption. These pink hues are associated with the oxidation of magnetite nanolites in the presence of air at high temperatures, serving as an indicative sign of a sub-aerial eruptive column, as discussed in Knafelc et al., 2022. Thus, in order to establish a more comprehensive relationship, it is imperative to investigate the correlation between color indicators and magnetic parameters in additional sets of pumices.

6 | CONCLUSIONS

1. The magnetic carrier present in all the samples is Ti-magnetite exhibiting a constant level of substitution and characterized by the general formula: $\text{Fe}_{2.6} \text{M}_y \text{Ti}_x \text{O}_4$ where M corresponds to a mixture of variable proportion of Al and Mg with $x + y \sim 0.4$.
2. The magnetic hysteresis properties and FORC diagrams, which are strongly influenced by the size of iron oxide crystals, exhibit similarities among the pumices of similar color. However, they show pronounced differences when comparing pumices of different colors. This contrast suggests that the iron oxides within the FOB samples are at varying stages of the nucleation, growth, and diffusion processes. Pumices from the lighter colors are associated with

a high concentration of small-sized iron oxide nanolites, expected to be in ESION range (below 3 nm). Pumices exhibiting the darker color are characterized by larger iron oxide crystals, with sizes from the SP-SD threshold (around 30 nm) up to a few hundred nanometers. In this last case, the iron oxides tend to be grouped together in crystal rich areas suggesting that diffusion occurred.

3. A strong correlation is established between the lightness of the pumices, determined using the HSL color format, and the concentrations of iron oxides within the glassy matrix.
4. All these observations align with a scenario in which the crystallization of nanolites occurred in the form of ESION within part of the magma chamber. Locally, conditions have allowed the growth of larger iron oxides giving rise to the SD population observed in BT pumices. In other regions, the crystals did not undergo significant growth, as evidenced by the characteristics of AT samples. Finally, in the PGT pumices it is shown that diffusion have played a central role with formation of patches rich in larger iron oxides reaching a few hundreds nm.
5. The magma is not re-equilibrated during eruption (see also discussion in Yoshida et al., 2023) and mixing occurs in the eruption conduit giving the observed BT and GT alternation in some pumices, at this point a degassing takes place as witnessed by the bubbles at the interface.
6. We infer that hysteresis parameters, coercivity and FORC analyses can be powerful means to better understand eruption dynamic during Plinian events. Our results along with study by Knafelc et al. (2022) show that magnetic analyses can help to trace magnetite nanolite nucleation and oxidation state and assess their importance in the initiation of explosive eruptions.
7. Finally, to comply with a FAIR approach, all the results from this study are made available in a data redepository: <https://doi.org/10.18715/IPGP.2023.lndb1d3z>.

ACKNOWLEDGMENTS

We thank Charles Lelosg and Nobuaki Fuji for discussions, and IPGP and CNRS for fundings. KY thanks JSPS KAKENHI, grant No. JP19K14825, Funding institution: Japan Society for the Promotion of Science. We are grateful to E. Ferré and one anonymous reviewer for the very interesting questions they raised which helped to improve the manuscript.

FUNDING INFORMATION

We thank Centre National de la Recherche Scientifique and Institut de Physique du Globe de Paris for general fundings. KY thanks JSPS KAKENHI, grant no. JP19K14825, Japan Society for the Promotion of Science.

CONFLICT OF INTEREST STATEMENT

The authors declare no conflict of interest.

ORCID

Julie Carlut  <https://orcid.org/0000-0002-4493-8530>

Aude Isambert  <https://orcid.org/0009-0004-4720-4059>

Claire Carvallo  <https://orcid.org/0000-0002-0986-3203>

Geoffrey Garcia da Fonseca  <https://orcid.org/0009-0002-9757-5523>

Nelly-Wangue Moussissa  <https://orcid.org/0009-0009-3062-8425>

Kenta Yoshida  <https://orcid.org/0000-0001-9525-1598>

REFERENCES

- Akimoto, S. I., Katsura, T., & Yoshida, M. (1957). Magnetic properties of TiFe_2O_4 - Fe_3O_4 system and their change with oxidation. *Journal of Geomagnetism and Geolectricity*, 9(4), 165–178.
- Butler, R. F., & Banerjee, S. K. (1975). Theoretical single-domain grain size range in magnetite and titanomagnetite. *Journal of Geophysical Research*, 80(29), 4049–4058.
- Clark, D. A. (1997). Magnetic petrophysics and magnetic petrology: Aids to geological interpretation of magnetic surveys. *Journal of Australian Geology and Geophysics*, 17(2), 83–103.
- Day, R., Fuller, M., & Schmidt, V. A. (1977). Hysteresis properties of titanomagnetites: Grain-size and compositional dependence. *Physics of the Earth and Planetary Interiors*, 13(4), 260–267.
- Di Genova, D., Brooker, R. A., Mader, H. M., Drewitt, J. W., Longo, A., Deubener, J., Neuville, D., Fanara, S., Shebanova, O., Anzellini, S., Arzilli, F., Bamber, E. C., Hennet, L., La Spina, G., & Miyajima, N. (2020). In situ observation of nanolite growth in volcanic melt: A driving force for explosive eruptions. *Science Advances*, 6(39), eabb0413.
- Egli, R. (2003). Analysis of the field dependence of remanent magnetization curves. *Journal of Geophysical Research: Solid Earth*, 108(B2).
- Egli, R. (2013). VARIFORC: An optimized protocol for calculating non-regular first-order reversal curve (FORC) diagrams. *Global and Planetary Change*, 110, 302–320.
- Harrison, R. J., & Feinberg, J. M. (2008). FORCinel: An improved algorithm for calculating first order reversal curve distributions using locally weighted regression smoothing. *Geochemistry, Geophysics, Geosystems*, 9(5).
- Heslop, D., McIntosh, G., & Dekkers, M. J. (2004). Using time- and temperature-dependent Preisach models to investigate the limitations of modelling isothermal remanent magnetization acquisition curves with cumulative log Gaussian functions. *Geophysical Journal International*, 157(1), 55–63.
- Jiang, Z., Liu, Q., Zhao, X., Roberts, A. P., Heslop, D., Barrón, V., & Torrent, J. (2016). Magnetism of Al-substituted magnetite reduced from Al-hematite. *Journal of Geophysical Research: Solid Earth*, 121(6), 4195–4210. <https://doi.org/10.1002/2016jb012863>
- Kim, B. H., Lee, N., Kim, H., An, K., Park, Y. I., Choi, Y., & Hyeon, T. (2011). Large-scale synthesis of uniform and extremely small-sized iron oxide nanoparticles for high-resolution T1 magnetic resonance imaging contrast agents. *Journal of the American Chemical Society*, 133(32), 12624–12631. <https://doi.org/10.1021/ja203340u>
- Knafelc, J., Bryan, S. E., Jones, M. W., Gust, D., Mallmann, G., Cathey, H. E., Berry, A. J., Ferré, E. C., & Howard, D. L. (2022). Havre 2012 pink pumice is evidence of a short-lived, deep-sea, magnetite nanolite-driven explosive eruption. *Communications Earth & Environment*, 3(1), 19.
- Kruiver, P. P., Dekkers, M. J., & Heslop, D. (2001). Quantification of magnetic coercivity components by the analysis of acquisition curves of isothermal remanent magnetisation. *Earth and Planetary Science Letters*, 189(3–4), 269–276.
- Linderoth, S., Hendriksen, P. V., Bødker, F., Wells, S., Davies, K., Charles, S. W., & Mørup, S. (1994). On spin-canting in maghemite particles. *Journal of Applied Physics*, 75(10), 6583–6585. <https://doi.org/10.1063/1.356902>
- Maeno, F., Kaneko, T., Ichihara, M., Suzuki, Y. J., Yasuda, A., Nishida, K., & Ohminato, T. (2022). Seawater-magma interactions sustained the high column during the 2021 phreatomagmatic eruption of Fukutoku-Oka-no-Ba. *Communications Earth & Environment*, 3(1), 260. <https://doi.org/10.1038/s43247-022-00594-4>
- Malvoisin, B., Carlut, J., & Brunet, F. (2012). Serpentinization of oceanic peridotites: 1. A high-sensitivity method to monitor magnetite production in hydrothermal experiments. *Journal of Geophysical Research: Solid Earth*, 117(B1).
- Maxbauer, D. P., Feinberg, J. M., & Fox, D. L. (2016). MAX UnMix: A web application for unmixing magnetic coercivity distributions. *Computers & Geosciences*, 95, 140–145.
- Mollo, S., Putirka, K., Iezzi, G., & Scarlato, P. (2013). The control of cooling rate on titanomagnetite composition: Implications for a geospeedometry model applicable to alkaline rocks from Mt. Etna volcano. *Contributions to Mineralogy and Petrology*, 165(3), 457–475. <https://doi.org/10.1007/s00410-012-0817-6>
- Muxworthy, A. R., & Williams, W. (2009). Critical superparamagnetic/single-domain grain sizes in interacting magnetite particles: Implications for magnetosome crystals. *Journal of the Royal Society Interface*, 6(41), 1207–1212.
- O'Reilly, W. (1984). *Rock and mineral magnetism*. Springer US. <https://doi.org/10.1007/978-1-4684-8468-7>
- Pike, C. R., Roberts, A. P., & Verosub, K. L. (1999). Characterizing interactions in fine magnetic particle systems using first order reversal curves. *Journal of Applied Physics*, 85, 6660–6667.
- Roberts, A., Pike, C., & Verosub, K. (2000). First-order reversal curve diagrams: A new tool for characterizing the magnetic properties of natural samples. *Journal of Geophysical Research Atmospheres*, 105, 28461–28475. <https://doi.org/10.1029/2000jb900326>
- Roberts, A. P., Cui, Y., & Verosub, K. L. (1995). Wasp-waisted hysteresis loops: Mineral magnetic characteristics and discrimination of components in mixed magnetic systems. *Journal of Geophysical Research: Solid Earth*, 100(B9), 17909–17924. <https://doi.org/10.1029/2000jb900326>
- Roca, A. G., Morales, M. P., O'Grady, K., & Serna, C. J. (2006). Structural and magnetic properties of uniform magnetite nanoparticles prepared by high temperature decomposition of organic precursors. *Nanotechnology*, 17(11), 2783–2788. <https://doi.org/10.1088/0957-4484/17/11/010>
- Tauxe, L., Mullender, T. A. T., & Pick, T. (1996). Potbellies, wasp-waists, and superparamagnetism in magnetic hysteresis. *Journal of Geophysical Research: Solid Earth*, 101(B1), 571–583.
- Wilkinson, M. D., Dumontier, M., Aalbersberg, I. J., Appleton, G., Axton, M., Baak, A., & Bourne, P. E. (2016). The FAIR guiding principles for scientific data management and stewardship. *Scientific Data*, 3(1), 1–9. <https://doi.org/10.1029/2000jb900326>
- Yoshida, K., Miyake, A., Okumura, S. H., Ishibashi, H., Okumura, S., Okamoto, A., Niwa, Y., Kimura, M., Sato, T., Tamura, Y., & Ono, S. (2023). Oxidation-induced nanolite crystallization triggered the 2021 eruption of Fukutoku-Oka-no-Ba, Japan. *Scientific Reports*, 13(1), 7117. <https://doi.org/10.1038/s41598-023-34301-w>
- Yoshida, K., Tamura, Y., Sato, T., Hanyu, T., Usui, Y., Chang, Q., & Ono, S. (2022). Variety of the drift pumice clasts from the 2021 Fukutoku-Oka-no-Ba eruption, Japan. *Island Arc*, 31(1), e12441. <https://doi.org/10.1111/iar.12441>

How to cite this article: Carlut, J., Isambert, A., Carvallo, C., Garcia da Fonseca, G., Moussissa, N.-W., Bouis, A., & Yoshida, K. (2024). Rock magnetic analyses as a tool to investigate diversity of drift pumice clasts: An example from Japan's 2021 Fukutoku-Oka-no-Ba (FOB) eruption. *Island Arc*, 33(1), e12507. <https://doi.org/10.1111/iar.12507>